

Calpain inhibition reduces ataxin-3 cleavage alleviating neuropathology and motor impairments in mouse models of Machado-Joseph disease

Ana Teresa Simões^{1,2}, Nélio Gonçalves^{1,2}, Rui Jorge Nobre¹, Carlos Bandeira Duarte^{1,3}, Luís Pereira de Almeida^{1,2,*}

¹CNC - Center for Neuroscience and Cell Biology, University of Coimbra, 3004-517 Coimbra, Portugal

²Faculty of Pharmacy, University of Coimbra, 3000-548 Coimbra, Portugal

³Faculty of Sciences and Technology, Department of Life Sciences, University of Coimbra, 3001-401 Coimbra, Portugal

*To whom correspondence address should be addressed at: Prof. Luís Pereira de Almeida, CNC - Center for Neuroscience and Cell Biology, University of Coimbra, Largo Marquês de Pombal, 3004-517 Coimbra, Portugal, Phone: +351 96 633 74 82, Fax: +351 239 853 409, E-mail: luispa@cnc.uc.pt or luispa@ci.uc.pt

ABSTRACT

Machado-Joseph Disease (MJD) is the most prevalent autosomal dominantly-inherited cerebellar ataxia. It is caused by an expanded CAG repeat in the *ATXN3* gene, which translates into a polyglutamine tract within the ataxin-3 protein. Present treatments are symptomatic and do not prevent disease progression. As calpain overactivation has been shown to contribute to mutant ataxin-3 proteolysis, translocation to the nucleus, inclusions formation and neurodegeneration, we investigated the potential role of calpain inhibition as a therapeutic strategy to alleviate MJD pathology. For this purpose, we administered orally the calpain inhibitor BDA-410 to a lentiviral mouse model of MJD.

Western-blot and immunohistochemical analysis revealed the presence of N- and C-terminal mutant ataxin-3 fragments and the colocalization of large inclusions with cleaved caspase-3 in the mice brain. Oral administration of the calpain inhibitor BDA-410 decreased both fragments formation and full-length ataxin-3 levels, reduced aggregation of mutant ataxin-3 and prevented cell injury and striatal and cerebellar degeneration. Importantly, in correlation with the preserved cerebellar morphology, BDA-410 prevented motor behavioural deficits. In conclusion, BDA-410 alleviates Machado-Joseph neuropathology and may therefore be an effective therapeutic option for MJD.

INTRODUCTION

Machado-Joseph disease, also known as spinocerebellar ataxia type 3 (MJD/SCA3), is the most prevalent autosomal dominantly-inherited cerebellar ataxia (1-2). The diagnosis of MJD relies on the use of molecular genetic testing to detect an abnormal CAG trinucleotide repeat expansion in the respective *ATXN3* gene located on chromosome 14q32.1 and is suggested in individuals with progressive cerebellar ataxia and pyramidal signs as well as ophthalmoplegia, dystonia, action-induced facial and lingual fasciculation-like movements, and bulging eyes (3-4). Current treatment is symptomatic without preventing neuronal cell death or delaying age of onset. Therefore, identification of molecular pathways of disease is crucial to unravel potential therapeutic targets.

The neurotoxicity of MJD has been proposed to be ignited by a proteolytic event, a mechanism commonly designated as the toxic fragment hypothesis. Cleavage of mutant ataxin-3 into smaller toxic fragments, which are prone to aggregation and promote cellular dysfunction (5-7), coupled with mutant ataxin-3 localization within the cell nucleus (8-9) seem to be key issues for the induction of neurodegeneration. The aforementioned proteolytic cleavage of mutant ataxin-3 has been associated with the protease calpain activity in different models: i) in mouse neuroblastoma cells (Neuro2a) (10), ii) in patient – specific induced pluripotent stem cell (iPSC)-derived neurons (11), iii) by our group in the lentiviral mouse model (12) and iv) in a MJD transgenic mouse model (13). We have previously shown that calpain-mediated proteolysis promotes a) ataxin-3 translocation to the nucleus, b) aggregation, c) cell injury, d) neurodegeneration and e) further contribution to the depletion of the endogenous calpain-specific inhibitor calpastatin in Machado-Joseph disease models and human tissue (12). Accordingly, knocking out calpastatin in a MJD transgenic mouse model leads to a worsening of behavioural and neuropathological abnormalities (13), suggesting that calpastatin depletion, meaning the lack of the internal inhibitor regulator, would contribute to calpain dysregulation leading to a calcium homeostasis imbalance, influencing the rate of ataxin-3 proteolysis and the subsequent neurodegeneration process (12-16). Together, these studies strongly suggest that calpain inhibition may be a promising strategy to alleviate MJD.

Gene therapy with viral vectors for overexpression of calpastatin is particularly adequate and translatable to clinical setting to treat well-defined CNS regions. However, as the neuropathology of MJD involves multiple systems such as cerebellar systems, substantia nigra, cranial nerve motor nuclei (17-18), and the striatum (19-22), a strategy able to reach broader distribution, while minimizing invasiveness, such as an orally-administered low molecular weight drug is also needed either as a single or complementary therapy. Therefore, in this study, we investigated whether a novel and highly specific cysteine protease inhibitor termed BDA-410 (23-26) would alleviate MJD. Using a lentiviral mouse model of MJD (12, 19), we investigated whether this orally-administered compound mediated neuroprotection.

Our results show that BDA-410 inhibited calpain-mediated proteolysis and decreased mutant ataxin-3 aggregation. In addition, this calpain inhibitor prevented cell injury, degeneration in the mouse brain resulting in the alleviation of behavioural deficits, suggesting that it may provide a new therapeutic choice for MJD.

RESULTS

BDA-410 inhibits calpain activity and decreases mutant ataxin-3 levels in vitro

Several evidences indicate that calpains cleave ataxin-3 producing proteolytic fragments that trigger MJD pathology (10-13), suggesting that calpain inhibition may provide an effective therapy for MJD. Therefore, we first investigated whether calpains could be inhibited by the novel oral calpain inhibitor BDA-410 (Fig. 1A) (23-26), in cultures of cerebellar granule neurons.

When calcium concentration increases in the intracellular compartment, a subset of axonal structural proteins is vulnerable to calpain activity, including α II-spectrin, a potential biomarker for neuronal cell injury (27). Interestingly, levels of the calpain-generated 150/145 kDa fragments of α II-spectrin were further increased when cerebellar granule neurons were transduced with lentiviral vectors encoding the mutant ataxin-3 (ATX-3 72Q) in opposition to wild-type ataxin-3 (ATX-3 27Q) and non-infected cultures (\emptyset). Importantly, BDA-410 (50 and 100 nM) mediated a decrease of the α II-spectrin fragments in cultures expressing mutant ataxin-3 (Fig.

1B,D). Furthermore, this calpain inhibition translated into a significant 21% decrease in immunolabeling of full-length mutant ataxin-3 (Fig. 1C,E).

Since the concentration of BDA-410 used in this experiment was very low (50 and 100 nM), much below the required to inactivate other proteases than calpains (typically in the μ M range; see Materials and Methods section for IC50 information), we conclude that the decreased levels of mutant ataxin-3 are due to a specific calpain inhibitory action. As a consequence, a reduced calpain-mediated cleavage of ataxin-3 might prevent the full-length protein and its fragments from escaping the cytoplasmic quality control mechanisms.

BDA-410 reduces cleavage of mutant ataxin-3 in a lentiviral mouse model of MJD

Therefore, in order to investigate whether orally-administered BDA-410 would inhibit ataxin-3 cleavage *in vivo*, we daily administered the compound BDA-410 (30 mg/kg in 1% Tween80 saline in a volume equal to 5 ml/kg) by oral gavage to a lentiviral mouse model, wherein lentiviral vectors encoding for wild-type ataxin-3 (ATX-3 27Q) were injected in the left striatum hemisphere and mutant ataxin-3 (ATX-3 72Q) in the right hemisphere, a strategy that we use to generate models of disease (12, 19, 28-30). As a control, a group of animals received only the vehicle in which BDA-410 was resuspended for the treated group. After 4 weeks of treatment, mice were sacrificed and striatal tissue processed for western blot analysis.

Two ataxin-3 fragments of ~26 kDa and ~34 kDa were detected at high levels in the brain hemispheres expressing mutant ataxin-3, or less and not detected, respectively, in the brain hemispheres expressing wild-type ataxin-3 protein (Fig. 2A-C, arrowheads). In addition, the ~26 kDa fragment was detected using any of the 3 antibodies targeting ataxin-3 protein, namely: i) Ab 1H9 (Fig. 2A), which recognizes the human ataxin-3 fragment from amino acids E214-L233, ii) Ab 1C2 (Fig. 2B), an antibody specific for the polyQ stretch, present at ataxin-3 C-terminal, and iii) Ab myc (Fig. 2C), an antibody for a myc tag located at the N-terminal of the protein. In sum, the ~34 kDa fragment was only detected for the mutant protein and when using Ab 1H9 and Ab 1C2 (Fig. 2A-B), suggesting that while the ~26 kDa might be both a N- or C-terminal fragment, the ~34 kDa fragment is only C-terminal. Notably, calpains inhibition by BDA-410

administration significantly decreased by 50% and 37.6% the formation of the 26 kDa fragment of the wild-type and mutant ataxin-3, respectively (Fig. 2A,D). Furthermore, upon calpains inhibition, the levels of the ~34 kDa fragment despite not reaching significant difference ($p=0.068$) tended to decrease ($\cong 22.5\%$, Fig. 2A,E).

However, as we observed a general decrease of the different ataxin-3 species: aggregates (Fig. 2A, 3G), fragments (Fig. 2D-E) and even a slight decrease of full-length (Fig. 2F), we hypothesized whether inhibition at the transcription level could be occurring. RNA extraction was then performed using the same experimental paradigm. Real time PCR confirmed that the decreased fragmentation is not a consequence of a decreased mRNA expression, indicating that the reduction of mutant ataxin-3 fragment levels was not due to inhibition of transcription.

BDA-410 inhibits mutant ataxin-3 aggregation in vivo by decreased fragmentation

To investigate if reduced calpain-mediated production of fragments by BDA-410 would prevent the subsequent phenomena predicted by the toxic fragment hypothesis, namely seeding of intranuclear inclusions and neurodegeneration (5-7, 10-12), we performed a similar experiment but now sacrificing the mice at a later time point (8 weeks post-injection) and processing the brains for immunohistochemistry.

Vehicle group transduced with ATX-3 72Q displayed a large number of mutant ataxin-3 (Fig. 3A,C) and ubiquitin (Fig. 3E) inclusions. Daily oral gavage of the calpain inhibitor during 8 weeks promoted a 38% significant decrease in the number of mutant ataxin-3 inclusions (Fig. 3A-D,G) and a similar tendency regarding the number of ubiquitinated inclusions (Fig. 3E-F). No alteration was observed between treated and vehicle groups when ATX-3 27Q was expressed (Fig. S1A-F). These results support the idea that ataxin-3 cleavage by calpains is required for the subsequent aggregation process and that calpain inhibition can reduce mutant ataxin-3 aggregation by suppressing the formation of toxic cleavage fragments.

Mutant ataxin-3 aggregates of specific size have different toxic properties

To clarify these findings, we further analyzed the size of mutant ataxin-3 aggregates and correlated with cytotoxicity by evaluation of cleaved caspase-3 immunoreactivity, an end-stage effector of apoptotic cell death. Calpains inhibition by BDA-410 administration mediated a small decrease in aggregates size of 0.22 μm (Fig. 4A-F,M). Even though fragments and soluble oligomers are thought to be the toxic species and contribute to aggregation (6), we found that larger aggregates (mean diameter: 4 μm) co-localized significantly more with cleaved caspase-3 than smaller aggregates (mean diameter: 1.6 μm) (Fig. 4G-L,N) for both groups. However, upon calpains inhibition, the number of mutant ataxin-3 positive cells co-expressing cleaved caspase-3 significantly decreased by 14% (Fig. 4G-L,O). Interestingly, in common cases where mutant ataxin-3 remained perinuclear, such as the representative cell pointed with an arrow in Fig. 4L, no cleaved caspase-3 immunoreactivity was observed suggesting that ataxin-3 nuclear localization is necessary for caspase-3 activation. These results show that mutant ataxin-3 aggregates of specific size have different toxic properties and suggest that BDA-410-mediated calpain inhibition decreases fragmentation, mutant ataxin-3 seeding and aggregation, with a small effect in aggregates size but promoting an important decrease in cytotoxicity.

BDA-410 mediates neuroprotection

To confirm that BDA-410 mediates neuroprotection, we monitored the effects of its oral administration over neuronal dysfunction, which may precede degeneration and clinical symptoms induced by mutant ataxin-3 (31). In this sense, we performed an immunohistochemical analysis for DARPP-32, a regulator of dopamine receptor signaling (32), as we have previously shown that it is a sensitive marker to detect early neuronal dysfunction (19, 28). Accordingly, the volume of the region depleted of DARPP-32 immunoreactivity was robustly and significantly reduced by 46% in the treated group when compared to the vehicle group (Fig. 5A-D,G).

Additionally, cresyl violet-stained sections further demonstrated that calpain inhibition promoted a significant reduction of 30% in the number of shrunken hyperchromatic nuclei (Fig. 5E-F,H), induced by mutant ataxin-3 expression in the brain of adult mice. No loss of DARPP-32 staining or increase of degenerated shrunken hyperchromatic nuclei was observed in the

hemispheres of mice expressing ATX-3 27Q treated or not with the calpains inhibitor compound (Fig. S1G-J).

Overall, these results are indicative of a neuroprotective effect provided by BDA-410 in a genetic mouse model of Machado-Joseph disease.

BDA-410 alleviates motor disabilities

To analyze if the neuroprotection mediated by BDA-410 would be translatable to an improved phenotype, motor behaviour was assessed in a cerebellar lentiviral model of MJD that presents extensive motor deficits induced by lentiviral-mediated expression of mutant ataxin-3 in the cerebellum (33). Non-injected mice (\emptyset) of the same age were used as a control.

Fine motor coordination was evaluated using a beam-walking test, which essentially examines the ability of mice to remain upright and to walk on an elevated and narrow beam without falling. Therefore, four beams of increasing difficulty of square and round cross-section were used and the time mice spent to cross them in order to reach an enclosed safety platform was recorded. Mice expressing ATX-3 72Q spent more time to cross the elevated beams along with a progressive walking disability accompanying an increasing beam difficulty. Calpain inhibition by BDA-410 administration significantly improved performance of animals (Fig. 6A).

To further realize whether a modulation of the neuromuscular transmission would be operated by calpain inhibition, a grip strength test was performed. Initially, all mice displayed equal muscle strength, but within the following 10 weeks post-injection, ATX-3 72Q promoted loss of strength that was prevented by BDA-410 administration (Fig. 6B). Finally, quantitative analysis of footprint pattern revealed tendency for shorter stride length in mice injected with ATX-3 72Q at 10 weeks post-injection that could be slightly ameliorated by calpains inhibition (Fig. 6C).

Taken together, fine motor function deterioration and grip strength loss were alleviated with the use of the calpain inhibitor BDA-410.

BDA-410 prevents cell loss

To determine whether the phenotypic modifications were due to cerebellar morphological preservation, several parameters in the transduced region were analyzed: lobule V volume (Fig. 7A-C,J), molecular layer thickness (Fig. 7D-F,K) and number of Purkinje cells (Fig. 7G-I,L).

To examine lobule V volume, cresyl violet-stained cross sectional areas were used for volume extrapolation. Mice injected with lentiviral vectors encoding for ATX-3 72Q and administered with vehicle exhibited a significant 61% reduction of lobule V volume. Calpain inhibition by BDA-410 oral administration was able to prevent 25% of the decreased volume (Fig. 7A-C,J).

In order to associate the cerebellar reduction with morphological modifications of specific cellular layers, cresyl violet-stained sections were also used to measure the molecular layer thickness. At 13 weeks post-injection, vehicle mice presented a significant two third reduction of the molecular layer thickness of lobule V. Oral administration of BDA-410 was able to prevent the aforementioned decrease to one third (Fig. 7D-F,K).

Immunofluorescence labelling of cerebellar sections with an anti-calbindin antibody revealed that vehicle mice displayed 87% reduction of Purkinje cell number and that administration of the calpain inhibitor BDA-410 protected 39% of the cell loss (Fig. 7G-I,L).

Overall, these data provide evidence that BDA-410 might contribute to morphological homeostasis leading ultimately to an improved phenotype.

DISCUSSION

Present treatment of Machado-Joseph disease is only supportive and no medication has been able to slow the course of disease. There is an urgent need for a disease-modifying therapy. The recent identification of the role of calpains in Machado-Joseph disease pathogenesis provided the rationale to the use of the calpain inhibitor BDA-410, which we show in the present work to robustly alleviate the neuropathology and motor deficits in a mouse model of this disorder.

Growing evidence suggests that calcium signalling is deranged in MJD (14), which coupled to decreased levels of the endogenous inhibitor of calpains – calpastatin (12), creates

favourable conditions for activation of these calcium-dependent cysteine proteases, proteolysis of mutant ataxin-3, generation of toxic fragments, translocation to the nucleus, aggregation and neurodegeneration (10-13). We have recently shown that calpastatin overexpression by viral gene therapy alleviated MJD neuropathology, providing the proof of principle that inhibition of calpains may be a potential new target for therapy of MJD (12). Therefore, in this study we investigated whether the oral compound BDA-410 (23-26) would be able to block calpain-mediated cleavage of ataxin-3 and alleviate MJD.

We found that BDA-410 reduced cleavage of the calpain natural substrate α -spectrin in cultures of cerebellar granule neurons only expressing mutant ataxin-3 (Fig. 1B,D), confirming its calpain inhibitory activity. Interestingly, in the same in vitro model, calpain inhibition was translated into a decrease in immunolabeling of full-length mutant ataxin-3 (Fig. 1C,E), which might be explained by a better clearance of mutant ataxin-3 by normal quality control mechanisms, preventing further accumulation of the non-cleaved full-length ataxin-3 through clearance by the UPS and autophagy-lysosomal pathways (29, 34).

According to the toxic fragment hypothesis, the aggregation process associated with inclusion formation and cellular dysfunction is initiated by the proteolytic cleavage of the full-length polyQ-protein (5-7). We have therefore analyzed ataxin-3 fragmentation upon BDA-410 administration and we observed a significant reduction of the ~26 kDa fragment and a decreasing trend of the ~34 kDa fragment formation (Fig. 2). Real time PCR confirmed that the decreased fragmentation is not a consequence of a decreased mRNA expression. In fact, BDA-410 was able to suppress mutant ataxin-3 proteolysis by calpains independently of mRNA levels of mutant ataxin-3 (data not shown). Cleavage of mutant ataxin-3 at amino acid 259 might lead to the formation of a N-terminal (Fig. 2C) and a C-terminal (Fig. 2B) fragments of ~26 kDa and ~34 kDa, respectively. Cleavage of mutant ataxin-3 before polyglutamine expansion might lead to the formation of a C-terminal (Fig. 2B) fragment of ~26 kDa. A simultaneous cleavage at amino acids 61 and 259 for both wild-type and mutant ataxin-3 might also give rise to the observed ~26 kDa fragment (Fig. 2A). Cleavage at amino acid 200 may generate a wild-type N and C-terminal fragments of ~26 kDa (Fig. 2A-C). The reduction of both the N- (35) and C- (7, 36) terminal

fragments formation of mutant ataxin-3 may have a contributive effect to neuroprotection mediated, in this study, by the calpain inhibitor BDA-410 (Fig. 2D-E).

BDA-410 mediated a reduction within the mouse brain of the number of mutant ataxin-3 intranuclear inclusions (Fig. 3), which are a hallmark of the pathology (37-39). We have previously shown that the diameter of mutant ataxin-3 inclusions decreased, as calpastatin levels increased (12). Even though BDA-410 had a minor effect in inclusions size (Fig. 4A-F,M), the number of mutant ataxin-3 positive cells co-expressing cleaved caspase-3 significantly decreased upon its administration, suggesting a neuroprotective role for the drug (Fig. 4G-L,O). Neuroprotection was further confirmed by a dramatic 46% decrease of the volume of the region depleted of DARPP-32 immunoreactivity and of the number of pycnotic nuclei in the treated group, when compared to the control group (Fig. 5). Importantly, BDA-410 was able to preserve cerebellar morphology (Fig. 7), one early target of the degenerative process of MJD (40).

On one hand, our results suggest that the fragments are the toxic species (Fig. 2) and that intranuclear inclusions might have a protective function, in agreement with the toxic fragment hypothesis (5-6, 30, 41). On the other hand, intranuclear inclusions do not solely comprise the polyglutamine protein. Functionally relevant proteins are sequestered such as ubiquitin (Fig. 4A-C), chaperones and proteasome components that are involved in quality control of protein surveillance machinery (42-44). Furthermore, inclusions might compromise cell integrity and disrupt axonal transport, through motor protein titration or physical interruption (45). Our studies thus demonstrate that despite being the fragments pernicious, larger aggregates present increased colocalization with cleaved caspase-3 (Fig. 4G-L, N) suggesting increased cytotoxicity as compared to smaller aggregates. Therefore, our results suggest that both theories might coexist. Nevertheless, BDA-410 is able to suppress fragmentation decreasing consequent aggregation.

Notably, this study demonstrates that calpain-mediated inhibition of the proteolytic event, allied with the neuroprotective effect can limit the worsening of the phenotype (Fig. 6). As MJD can be diagnosed by genetic testing, a therapeutic intervention, once available, might be initiated before the onset of symptoms, turning BDA-410 a viable choice.

Calpain inhibition might affect their physiological function and be consequently a matter of concern causing adverse side effects. However, calpastatin-deficient and transgenic mice did not present any defect in development, fertility, morphology or life span (15, 46). Moreover, under normal conditions, calpains cleave substrates at a limited number of sites leaving large and often catalytically active fragments, indicating that prior to a digestive function, calpains display a regulatory or signaling role (47). Thus, the occurrence of adverse side effects may be restricted. In fact, our results show neither alteration in subcellular localization of wild-type ataxin-3, nor cell injury or striatal degeneration (Fig. S1), upon BDA-410 administration.

In conclusion, the oral calpain inhibitor BDA-410 reduced fragmentation of mutant ataxin-3, decreased inclusion number, prevented cell injury and neurodegeneration and alleviated phenotypic impairment in a model of MJD. This study shows for the first time that a low molecular weight drug orally administered may provide a viable therapeutic option to block progression of MJD.

MATERIALS AND METHODS

Drug treatment

Calpain inhibitor BDA-410 was kindly provided by Dr. Hiroshi Kinoshita from Mitsubishi Tanabe Pharma Corporation, Yokohama, Japan. The chemical name of this compound is (2S)-N-(1S)-1-[(S)-Hydroxy(3-oxo-2-phenyl-1-cyclopropen-1-yl)methyl]-2-methylpropyl-2-benzenesulfonylamino-4-methylpentanamide (C₂₆H₃₂N₂O₅S; MW 484.61). BDA-410 has a potent and selective inhibitory action against calpains: calpain 1/calpain 2, IC₅₀ = 21.4 nM; papain, IC₅₀ = 400 nM; cathepsin B, IC₅₀ = 16 μM; thrombin, IC₅₀ >100 μM; cathepsin G, IC₅₀ >100 μM; cathepsin D, IC₅₀ = 91.2 μM; proteasome 20S, IC₅₀ >100 μM.

BDA-410 was orally administered (30 mg/kg in 1% Tween 80 saline in a volume equal to 5 ml/kg), with a 20G gavage needle, every day since two days before stereotaxic injection until sacrifice.

Cultures of cerebellar granule neurons

Primary cultures of rat cerebellar granule neurons were prepared from P7 post-natal Wistar rat pups. Cerebella were dissected and dissociated with trypsin (0.01%, 15 min, and 37°C, Sigma, T0303) and DNase (0.045 mg/ml, Sigma, D5025) in Ca²⁺- and Mg²⁺- free Krebs buffer (120 mM NaCl, 5 mM KCl, 1.2 mM KH₂PO₄, 13 mM glucose, 15 mM HEPES, 0.3% BSA, pH 7.4). Cerebella were then washed with Krebs buffer containing trypsin inhibitor (0.3 mg/ml, Sigma, T9128) to stop trypsin activity. The cells were dissociated in this solution, centrifuged and then resuspended in Basal Medium Eagle supplemented with 25 mM KCl, 30 mM glucose, 26 mM NaHCO₃, 1% penicillin-streptomycin (100 U/ml, 100 µg/ml) and 10% fetal bovine. Cells were plated on 6 or 12-well plates (1x10⁶ or 5x10⁵ cells/well) coated with poly-D-lysine. Cultures were maintained for 3 weeks in a humid incubator (5% CO₂/ 95% air at 37°C).

Animals

4-week-old C57BL/6J mice (Charles River) were used. The animals were housed in a temperature-controlled room maintained on a 12 h light / 12 h dark cycle. Food and water were provided *ad libitum*. The experiments were carried out in accordance with the European Union Directive 2010/63/EU covering the protection of animals used for scientific purposes.

Viral vectors production

Lentiviral vectors encoding human wild-type ataxin-3 (ATX-3 27Q) or mutant ataxin-3 (ATX-3 72Q) (19) were produced in 293T cells with a four-plasmid system, as previously described (48). The lentiviral particles were resuspended in 1% bovine serum albumin (BSA) in phosphate-buffered saline (PBS). The viral particle content of batches was determined by

assessing HIV-1 p24 antigen levels (RETROtek, Gentaur, Paris, France). Viral stocks were stored at -80°C until use.

Lentiviral infection of cerebellar granule neurons

The cell cultures were infected with lentiviral vectors at ratio of 10 ng of p24 antigen/ 10⁵ cells 1 day after plating (1 DIV) (49). At 2 DIV, medium was replaced with freshly prepared culture medium and calpain inhibitor BDA-410 was added in two different concentrations (50 and 100 nM in DMSO). DMSO was used as a control. Medium plus inhibitor or DMSO was replaced every three days.

In vivo injection in the striatum and cerebellum

Concentrated viral stocks were thawed on ice. Lentiviral vectors encoding human wild-type (ATX-3 27Q) or mutant ataxin-3 (ATX-3 72Q) were stereotaxically injected into the striatum in the following coordinates: anteroposterior: +0.6mm; medial-lateral: ±1.8mm; dorsoventral: -3.3mm; and into the cerebellum in the following coordinates: antero-posterior: -2.4mm; medial-lateral: 0mm; dorsoventral: -2.9mm. Animals were anesthetized by administration of avertin (200 µg/g, intraperitoneally).

For western-blot procedure and RNA extraction, wild-type mice received a single 2 µl injection of 0.3 mg of p24/ml lentivirus in each side: left hemisphere (ATX-3 27Q) and right hemisphere (ATX-3 72Q). For immunohistochemical procedure, wild-type mice received a single 1 µl injection of 0.4 mg of p24/ml lentivirus in each side: left hemisphere (ATX-3 27Q) and right hemisphere (ATX-3 72Q). Mice were kept in their home cages for 4 or 8 weeks, before being sacrificed for western-blot analysis and RNA extraction or immunohistochemical analysis, respectively.

For behavioural analysis and cerebellar morphologic assessment, wild-type mice received a single 4 μ l injection of 0.25 mg of p24/ml lentivirus encoding ATX-3 72Q. Non-injected mice (\emptyset) of the same age were used as a control.

Behavioural assessments

Mice were subjected to locomotor tests starting at 4 weeks of age. Animals were habituated for 1h to a quiet room with controlled temperature and ventilation, dimmed lighting, and handled prior to behavioural testing to overcome the animals' natural fear and anxiety responses, which could have a major effect on performance. All devices were wiped clean with a damp cloth of a 10% ethanol solution and dried before evaluating the next mouse.

Beam balance/walking. Motor coordination and balance of mice were assessed by measuring the ability of the mice to traverse a graded series of narrow beams to reach an enclosed safety platform (50). The beams consisted of long strips of wood (1-m) with an 18- or 9-mm square wide and a 9- or 6-mm round diameter cross-sections. The beams were placed horizontally, 25-cm above the bench surface, with one end mounted on a narrow support and the other end attached to an enclosed box (20-cm square) into which the mouse could escape. A 60-W desk lamp was positioned above near the start of the beam to create an aversive stimulus (bright light) to induce mice to cross it. Mice performed two consecutive trials on each beam, progressing from the widest to the narrowest beam and the mean taken to analysis. The mean latency time each animal spent to cross all the beams was considered.

Grip strength. The mouse limb strength was measured as an indicator of neuromuscular function. The setup consisted of a 300-g metal grid, which was on a scale. The animal was hung with its forepaws on the central position of the grid. Its strength was determined as the weight pushed (g) from the scale. The grip test was performed 3 times and the mean taken to analysis. Mice body weight was used as a normalization factor.

Footprint test. Gait analysis was assessed by the footprint test. To obtain footprints, the hindfeet and forefeet of the mice were coated with black and white nontoxic paints, respectively. Mice were allowed to walk on a greenish paper along a 100x10x15 cm runway. Stride length was measured as the average distance of forward movement between each stride. A sequence of six consecutive steps for both hind and forefeet was chosen for evaluation. The mean of the twelve strides for each animal was considered.

Immunohistochemical procedure

After an overdose of avertin (2.5x 200 µg/g, i.p.), transcardial perfusion of the mice was performed with a phosphate solution followed by fixation with 4% paraphormaldehyde (PFA). The brains were removed and post-fixed in 4% PFA for 24h and cryoprotected by incubation in 25% sucrose/ phosphate buffer for 48 h. The brains were frozen, 25 µ m coronal striatal sections and 35 µ m midsagittal cerebellar sections were cut using a cryostat (LEICA CM3050 S) at -21°C. Slices throughout the entire brain regions were collected in anatomical series and stored in 48-well trays as free-floating sections in PBS supplemented with 0.05 µ M sodium azide. The trays were stored at 4°C until immunohistochemical processing.

Sections from injected mice were processed with the following primary antibodies: a mouse monoclonal anti-ataxin-3 antibody (1H9, 1:5000; Chemicon, Temecula, CA), recognizing the human ataxin-3 fragment from amino acids F112-L249; a rabbit polyclonal anti-ubiquitin antibody (Dako, 1:1000; Cambridgeshire, UK); and a rabbit anti-DARPP-32 antibody (1:1000; Chemicon, Temecula, CA), followed by incubation with the respective biotinylated secondary antibodies (1:200; Vector Laboratories). Bound antibodies were visualized using the Vectastain ABC kit, with 3,3'-diaminobenzidine tetrahydrochloride (DAB metal concentrate; Pierce) as substrate.

Double stainings for Ataxin-3 (1H9, 1:3000; Chemicon, Temecula, CA), nuclear marker (DAPI, blue) and ubiquitin (Dako, 1:1000; Cambridgeshire, UK), cleaved caspase-3 (Asp175,

1:2000; Cell Signaling) or calbindin (Ab1778, 1:500; Chemicon, Temecula, CA) were performed. Free-floating sections from injected mice were at RT for 2 h in PBS/0.1% Triton X-100 containing 10% NGS (Gibco), and then overnight at 4°C in blocking solution with the primary antibodies. Sections were washed three times and incubated for 2 h at RT with the corresponding secondary antibodies coupled to fluorophores (1:200; Molecular Probes, Oregon, USA) diluted in the respective blocking solution. The sections were washed three times and then mounted in Fluorsave Reagent[®] (Calbiochem, Germany) on microscope slides.

Staining was visualized using Zeiss Axioskop 2 plus, Zeiss Axiovert 200 and Zeiss LSM 510 Meta imaging microscopes (Carl Zeiss Microimaging, Germany), equipped with AxioCam HR color digital cameras (Carl Zeiss Microimaging) using 5x, 20x, 40x and 63x Plan-Neofluar and a 63x Plan/Apochromat objectives and the AxioVision 4.7 software package (Carl Zeiss Microimaging).

Cresyl violet staining

Premounted sections were stained with cresyl violet for 30 secs, differentiated in 70% ethanol, dehydrated by passing twice through 95% ethanol, 100% ethanol and xylene solutions, and mounted onto microscope slides with Eukitt[®] (Sigma).

Evaluation of the volume of the DARPP-32 depleted volume and lobule V volume

The extent of ataxin-3 lesions in the striatum or the cerebellar lobule V volume was analyzed by photographing, with a x1.25 objective, 8 DARPP-32 stained sections per animal (at 200 µm intervals) or 8 cerebellar cresyl violet sections per animal (at 210 µm intervals), selected so as to obtain complete sampling of the striatum or hemicerebellum, and by quantifying the area of the lesion or the lobule with a semiautomated image-analysis software package (Image J software, USA). The volume was then estimated with the following formula: volume =

$d(a_1+a_2+a_3 \dots)$, where d is the distance between serial sections and $a_1+a_2+a_3$ are the areas for individual serial sections.

Cell counts and morphometric analysis of ataxin-3 and ubiquitin inclusions, and lobule V molecular layer

Coronal sections showing complete rostrocaudal sampling (1 of 11 sections) of the striatum were scanned with a x20 objective. The analyzed areas of the striatum encompassed the entire region containing ATX-3 and ubiquitin inclusions, as revealed by staining with the anti-ataxin-3 and anti-ubiquitin antibodies. All inclusions were manually counted using a semiautomated image-analysis software package (Image J software, USA). Inclusions diameter was assessed by scanning the area above the needle tract in four different sections, using a x63 objective. At least 100 inclusions per animal were analyzed using LSM Image Browser. Inclusions diameter was further assessed by double staining of ataxin-3 inclusions with cleaved caspase-3 by scanning the area above the needle tract in three different sections, using a x63 objective. At least 100 inclusions per animal were analyzed using LSM Image Browser.

Midsagittal sections of hemiserebellum were scanned with a x20 objective. All calbindin-positive Purkinje cells of lobule V of 6 sections at 210 μm intervals were manually counted. Lobule V molecular layer thickness was assessed by the mean of four different measures. In each image, a boundary line around the molecular layer from, but excluding, the Purkinje cell bodies to the pial surface was drawn by hand using a semiautomated image-analysis software package (Image J software, USA).

Western-blot analysis

For assessment of ataxin-3 proteolysis in the lentiviral model of MJD, transcordial perfusion of the mice was performed with ice-cold phosphate buffered saline containing 10 mM EDTA and 10 mM of the alkylating reagent N-ethylmaleimide, to avoid post-mortem calpain

overactivation. The injected striata were then dissected and immediately sonicated in RIPA buffer (50 mM Tris-HCl, pH 7.4, 150 mM NaCl, 7 mM EDTA, 1% NP-40, 0.1% SDS, 10 μ g/ml DTT, 1mM PMSF, 200 μ g/ml leupeptin, protease inhibitors cocktail).

One week before cell lysis, cerebellar granule neurons were treated with 200 μ M NMDA plus 2.5 mM CaCl₂ in Krebs buffer without MgCl₂ for one hour for excitatory stimulation and subsequently cultured in fresh medium plus inhibitor or DMSO until harvest and sonication in RIPA buffer, as described above.

Equal amounts (20 μ g of protein) were resolved on 12% SDS-polyacrylamide gels and transferred onto PVDF membranes. Immunoblotting was performed using the monoclonal anti-ataxin-3 antibody (1H9, 1:1000; Chemicon, Temecula, CA), monoclonal anti-polyglutamine antibody (1C2, MAB1574, 1:1000; Chemicon), monoclonal anti-myc tag (clone 4A6, 1:1000; Cell Signaling), monoclonal anti-spectrin antibody (MAB1622, 1:1000; Chemicon) and monoclonal anti- β -actin (clone AC-74, 1:5000; Sigma) or monoclonal anti- β -tubulin I (clone SAP.4G5, 1:15000; Sigma). Semi-quantitative analysis was carried out using Quantity-one 1-D image analysis software version 4.5. A partition ratio with actin or tubulin was calculated.

Purification of total RNA from striata of mice and cDNA synthesis

Mice were sacrificed by cervical dislocation and injected striata were dissected and stored overnight at 4°C in tubes containing RNAlater RNA stabilization reagent (QIAGEN). Samples were then kept at -80°C until extraction of RNA. Total RNA was isolated using the RNeasy Mini Kit (QIAGEN) according to the manufacturer's instructions. Briefly, after cell lysis, the total RNA was adsorbed to a silica membrane, washed with the recommended buffers and eluted with 30 μ l of RNase-free water by centrifugation. Total amount of RNA was quantified by optical density (OD) using a Nanodrop 2000 Spectrophotometer (Thermo Scientific) and the purity was evaluated by measuring the ratio of OD at 260 and 280 nm. cDNA was then obtained by

conversion of 1 µg of total RNA using the iScript Select cDNA Synthesis Kit (Bio-Rad) according to the manufacturer's instructions and stored at -20°C .

Quantitative real-time polymerase chain reaction (qRT-PCR)

Quantitative PCR was performed in an iQ5 thermocycler (Bio-Rad) using 96-well microtitre plates and the QuantiTect SYBR Green PCR Master Mix (QIAGEN). The primers for the target human gene (ATXN3, NM_004993) and the reference mouse genes (Hprt, NM_013556 and Gapdh, NM_008084) were pre-designed and validated by QIAGEN (QuantiTect Primers, QIAGEN). A master mix was prepared for each primer set containing the appropriate volume of QuantiTect SYBR Green PCR Master Mix (QIAGEN), QuantiTect Primers (QIAGEN) and template cDNA. All reactions were performed in duplicate and according to the manufacturer's recommendations: 95°C for 15 min, followed by 40 cycles at 94°C for 15 sec, 55°C for 30 sec and 72°C for 30 sec. The amplification efficiency for each primer pair and the threshold values for threshold cycle determination (Ct) were determined automatically by the iQ5 Optical System Software (Bio-Rad). The mRNA fold increase or fold decrease with respect to control samples was determined by the Pfaffl method, taking into consideration different amplification efficiencies of all genes.

Statistical analysis

Statistical analysis was performed using unpaired Student's *t*-test or one-way ANOVA followed by Bonferroni test for selected pairs comparison. Values of $p \leq 0.05$ were considered statistically significant; $p < 0.01$ very significant; and $p < 0.001$ extremely significant.

ACKNOWLEDGEMENTS

The authors wish to thank Luísa Cortes from the CNC - MICC Imaging facility for image acquisition assistance on confocal microscopy. This work was supported by funds FEDER through the Competitive Factors Operational Program – COMPETE and by national funds through the Portuguese Foundation for Science and Technology, PTDC/SAU-NEU/099307/2008, PEst-C/SAU/LA0001/2013-2014 and Programa Mais Centro (CENTRO-07-ST24-FEDER-002002, 002006, 002008). Ana Teresa Simões, Nélío Gonçalves and Rui Jorge Nobre were supported by the Portuguese Foundation for Science and Technology, Fellowships SFRH/BPD/87341/2012, SFRH/BD/38636/2007 and SFRH/BPD/66705/2009.

CONFLICT OF INTEREST STATEMENT

The authors declare no conflict of interests.

REFERENCES

- 1 Schols, L., Bauer, P., Schmidt, T., Schulte, T. and Riess, O. (2004) Autosomal dominant cerebellar ataxias: clinical features, genetics, and pathogenesis. *Lancet Neurol.*, **3**, 291-304.
- 2 Ranum, L.P., Lundgren, J.K., Schut, L.J., Ahrens, M.J., Perlman, S., Aita, J., Bird, T.D., Gomez, C. and Orr, H.T. (1995) Spinocerebellar ataxia type 1 and Machado-Joseph disease: incidence of CAG expansions among adult-onset ataxia patients from 311 families with dominant, recessive, or sporadic ataxia. *Am. J. Hum. Genet.*, **57**, 603-608.
- 3 Lima, L. and Coutinho, P. (1980) Clinical criteria for diagnosis of Machado-Joseph disease: report of a non-Azorena Portuguese family. *Neurology*, **30**, 319-322.
- 4 D'Abreu, A., Franca, M.C., Jr., Paulson, H.L. and Lopes-Cendes, I. (2010) Caring for Machado-Joseph disease: current understanding and how to help patients. *Parkinsonism Relat. Disord.*, **16**, 2-7.
- 5 Haacke, A., Broadley, S.A., Boteva, R., Tzvetkov, N., Hartl, F.U. and Breuer, P. (2006) Proteolytic cleavage of polyglutamine-expanded ataxin-3 is critical for aggregation and sequestration of non-expanded ataxin-3. *Hum. Mol. Genet.*, **15**, 555-568.
- 6 Takahashi, T., Kikuchi, S., Katada, S., Nagai, Y., Nishizawa, M. and Onodera, O. (2008) Soluble polyglutamine oligomers formed prior to inclusion body formation are cytotoxic. *Hum. Mol. Genet.*, **17**, 345-356.
- 7 Ikeda, H., Yamaguchi, M., Sugai, S., Aze, Y., Narumiya, S. and Kakizuka, A. (1996) Expanded polyglutamine in the Machado-Joseph disease protein induces cell death in vitro and in vivo. *Nat. Genet.*, **13**, 196-202.
- 8 Yang, W., Dunlap, J.R., Andrews, R.B. and Wetzel, R. (2002) Aggregated polyglutamine peptides delivered to nuclei are toxic to mammalian cells. *Hum. Mol. Genet.*, **11**, 2905-2917.
- 9 Bichelmeier, U., Schmidt, T., Hubener, J., Boy, J., Ruttiger, L., Habig, K., Poths, S., Bonin, M., Knipper, M., Schmidt, W.J. *et al.* (2007) Nuclear localization of ataxin-3 is required for the manifestation of symptoms in SCA3: in vivo evidence. *J. Neurosci.*, **27**, 7418-7428.
- 10 Haacke, A., Hartl, F.U. and Breuer, P. (2007) Calpain inhibition is sufficient to suppress aggregation of polyglutamine-expanded ataxin-3. *J. Biol. Chem.*, **282**, 18851-18856.
- 11 Koch, P., Breuer, P., Peitz, M., Jungverdorben, J., Kesavan, J., Poppe, D., Doerr, J., Ladewig, J., Mertens, J., Tuting, T. *et al.* (2011) Excitation-induced ataxin-3 aggregation in neurons from patients with Machado-Joseph disease. *Nature*, **480**, 543-546.
- 12 Simões, A.T., Gonçalves, N., Koeppen, A., Déglon, N., Kügler, S., Duarte, C.B. and Pereira de Almeida, L. (2012) Calpastatin-mediated inhibition of calpains in the mouse brain prevents mutant ataxin 3 proteolysis, nuclear localization and aggregation, relieving Machado-Joseph disease. *Brain*, **135**, 2428-2439.
- 13 Hubener, J., Weber, J.J., Richter, C., Honold, L., Weiss, A., Murad, F., Breuer, P., Wullner, U., Bellstedt, P., Paquet-Durand, F. *et al.* (2013) Calpain-mediated ataxin-3 cleavage in the molecular pathogenesis of spinocerebellar ataxia type 3 (SCA3). *Hum. Mol. Genet.*, **22**, 508-518.
- 14 Chen, X., Tang, T.S., Tu, H., Nelson, O., Pook, M., Hammer, R., Nukina, N. and Bezprozvanny, I. (2008) Deranged calcium signaling and neurodegeneration in spinocerebellar ataxia type 3. *J. Neurosci.*, **28**, 12713-12724.

- 15 Takano, J., Tomioka, M., Tsubuki, S., Higuchi, M., Iwata, N., Itoharu, S., Maki, M. and Saido, T.C. (2005) Calpain mediates excitotoxic DNA fragmentation via mitochondrial pathways in adult brains: evidence from calpastatin mutant mice. *J. Biol. Chem.*, **280**, 16175-16184.
- 16 Rao, M.V., Mohan, P.S., Peterhoff, C.M., Yang, D.S., Schmidt, S.D., Stavrides, P.H., Campbell, J., Chen, Y., Jiang, Y., Paskevich, P.A. *et al.* (2008) Marked calpastatin (CAST) depletion in Alzheimer's disease accelerates cytoskeleton disruption and neurodegeneration: neuroprotection by CAST overexpression. *J. Neurosci.*, **28**, 12241-12254.
- 17 Durr, A., Stevanin, G., Cancel, G., Duyckaerts, C., Abbas, N., Didierjean, O., Chneiweiss, H., Benomar, A., Lyon-Caen, O., Julien, J. *et al.* (1996) Spinocerebellar ataxia 3 and Machado-Joseph disease: clinical, molecular, and neuropathological features. *Ann. Neurol.*, **39**, 490-499.
- 18 Sudarsky, L. and Coutinho, P. (1995) Machado-Joseph disease. *Clin. Neurosci.*, **3**, 17-22.
- 19 Alves, S., Regulier, E., Nascimento-Ferreira, I., Hassig, R., Dufour, N., Koeppen, A., Carvalho, A.L., Simoes, S., de Lima, M.C., Brouillet, E. *et al.* (2008) Striatal and nigral pathology in a lentiviral rat model of Machado-Joseph disease. *Hum. Mol. Genet.*, **17**, 2071-2083.
- 20 Taniwaki, T., Sakai, T., Kobayashi, T., Kuwabara, Y., Otsuka, M., Ichiya, Y., Masuda, K. and Goto, I. (1997) Positron emission tomography (PET) in Machado-Joseph disease. *J. Neurol. Sci.*, **145**, 63-67.
- 21 Wullner, U., Reimold, M., Abele, M., Burk, K., Minnerop, M., Dohmen, B.M., Machulla, H.J., Bares, R. and Klockgether, T. (2005) Dopamine transporter positron emission tomography in spinocerebellar ataxias type 1, 2, 3, and 6. *Arch. Neurol.*, **62**, 1280-1285.
- 22 Klockgether, T., Skalej, M., Wedekind, D., Luft, A.R., Welte, D., Schulz, J.B., Abele, M., Burk, K., Laccone, F., Brice, A. *et al.* (1998) Autosomal dominant cerebellar ataxia type I. MRI-based volumetry of posterior fossa structures and basal ganglia in spinocerebellar ataxia types 1, 2 and 3. *Brain*, **121**, 1687-1693.
- 23 Li, X., Chen, H., Jeong, J.J. and Chishti, A.H. (2007) BDA-410: a novel synthetic calpain inhibitor active against blood stage malaria. *Mol. Biochem. Parasitol.*, **155**, 26-32.
- 24 Trinchese, F., Fa, M., Liu, S., Zhang, H., Hidalgo, A., Schmidt, S.D., Yamaguchi, H., Yoshii, N., Mathews, P.M., Nixon, R.A. *et al.* (2008) Inhibition of calpains improves memory and synaptic transmission in a mouse model of Alzheimer disease. *J. Clin. Invest.*, **118**, 2796-2807.
- 25 Subramanian, V., Uchida, H.A., Ijaz, T., Moorleggen, J.J., Howatt, D.A. and Balakrishnan, A. (2012) Calpain inhibition attenuates angiotensin II-induced abdominal aortic aneurysms and atherosclerosis in low-density lipoprotein receptor-deficient mice. *J. Cardiovasc. Pharmacol.*, **59**, 66-76.
- 26 Subramanian, V., Moorleggen, J.J., Balakrishnan, A., Howatt, D.A., Chishti, A.H. and Uchida, H.A. (2013) Calpain-2 compensation promotes angiotensin II-induced ascending and abdominal aortic aneurysms in calpain-1 deficient mice. *PLoS One*, **8**, e72214.
- 27 Liu, J., Liu, M.C. and Wang, K.K. (2008) Calpain in the CNS: from synaptic function to neurotoxicity. *Sci. Signal*, **1**, re1.
- 28 de Almeida, L.P., Ross, C.A., Zala, D., Aebischer, P. and Deglon, N. (2002) Lentiviral-mediated delivery of mutant huntingtin in the striatum of rats induces a

- selective neuropathology modulated by polyglutamine repeat size, huntingtin expression levels, and protein length. *J. Neurosci.*, **22**, 3473-3483.
- 29 Nascimento-Ferreira, I., Santos-Ferreira, T., Sousa-Ferreira, L., Auregan, G., Onofre, I., Alves, S., Dufour, N., Colomer Gould, V.F., Koeppen, A., Deglon, N. *et al.* (2011) Overexpression of the autophagic beclin-1 protein clears mutant ataxin-3 and alleviates Machado-Joseph disease. *Brain*, **134**, 1400-1415.
- 30 Gonçalves, N., Simões, A.T., Cunha, R.A. and Pereira de Almeida, L. (2013) Caffeine and adenosine A_{2A} receptor inactivation decrease striatal neuropathology in a lentiviral-based model of Machado-Joseph disease. *Ann. Neurol.*, **73**, 655-666.
- 31 Yen, T.C., Tzen, K.Y., Chen, M.C., Chou, Y.H., Chen, R.S., Chen, C.J., Wey, S.P., Ting, G. and Lu, C.S. (2002) Dopamine transporter concentration is reduced in asymptomatic Machado-Joseph disease gene carriers. *J. Nucl. Med.*, **43**, 153-159.
- 32 Greengard, P., Allen, P.B. and Nairn, A.C. (1999) Beyond the dopamine receptor: the DARPP-32/protein phosphatase-1 cascade. *Neuron*, **23**, 435-447.
- 33 Nobrega, C., Nascimento-Ferreira, I., Onofre, I., Albuquerque, D., Conceicao, M., Deglon, N. and de Almeida, L.P. (2013) Overexpression of mutant ataxin-3 in mouse cerebellum induces ataxia and cerebellar neuropathology. *Cerebellum*, **12**, 441-455.
- 34 Breuer, P., Haacke, A., Evert, B.O. and Wullner, U. (2010) Nuclear aggregation of polyglutamine-expanded ataxin-3: fragments escape the cytoplasmic quality control. *J. Biol. Chem.*, **285**, 6532-6537.
- 35 Hubener, J., Vauti, F., Funke, C., Wolburg, H., Ye, Y., Schmidt, T., Wolburg-Buchholz, K., Schmitt, I., Gardyan, A., Driessen, S. *et al.* (2011) N-terminal ataxin-3 causes neurological symptoms with inclusions, endoplasmic reticulum stress and ribosomal dislocation. *Brain*, **134**, 1925-1942.
- 36 Goti, D., Katzen, S.M., Mez, J., Kurtis, N., Kiluk, J., Ben-Haiem, L., Jenkins, N.A., Copeland, N.G., Kakizuka, A., Sharp, A.H. *et al.* (2004) A mutant ataxin-3 putative-cleavage fragment in brains of Machado-Joseph disease patients and transgenic mice is cytotoxic above a critical concentration. *J. Neurosci.*, **24**, 10266-10279.
- 37 Paulson, H.L., Perez, M.K., Trottier, Y., Trojanowski, J.Q., Subramony, S.H., Das, S.S., Vig, P., Mandel, J.L., Fischbeck, K.H. and Pittman, R.N. (1997) Intranuclear inclusions of expanded polyglutamine protein in spinocerebellar ataxia type 3. *Neuron*, **19**, 333-344.
- 38 Schmidt, T., Landwehrmeyer, G.B., Schmitt, I., Trottier, Y., Auburger, G., Laccone, F., Klockgether, T., Volpel, M., Epplen, J.T., Schols, L. *et al.* (1998) An isoform of ataxin-3 accumulates in the nucleus of neuronal cells in affected brain regions of SCA3 patients. *Brain Pathol.*, **8**, 669-679.
- 39 Yamada, M., Hayashi, S., Tsuji, S. and Takahashi, H. (2001) Involvement of the cerebral cortex and autonomic ganglia in Machado-Joseph disease. *Acta Neuropathol.*, **101**, 140-144.
- 40 Riess, O., Rub, U., Pastore, A., Bauer, P. and Schols, L. (2008) SCA3: neurological features, pathogenesis and animal models. *Cerebellum*, **7**, 125-137.
- 41 Ratovitski, T., Gucek, M., Jiang, H., Chighladze, E., Waldron, E., D'Ambola, J., Hou, Z., Liang, Y., Poirier, M.A., Hirschhorn, R.R. *et al.* (2009) Mutant huntingtin N-terminal fragments of specific size mediate aggregation and toxicity in neuronal cells. *J. Biol. Chem.*, **284**, 10855-10867.
- 42 Chai, Y., Berke, S.S., Cohen, R.E. and Paulson, H.L. (2004) Poly-ubiquitin binding by the polyglutamine disease protein ataxin-3 links its normal function to protein surveillance pathways. *J. Biol. Chem.*, **279**, 3605-3611.
- 43 Chai, Y., Koppenhafer, S.L., Shoosmith, S.J., Perez, M.K. and Paulson, H.L. (1999) Evidence for proteasome involvement in polyglutamine disease: localization to

nuclear inclusions in SCA3/MJD and suppression of polyglutamine aggregation in vitro. *Hum. Mol. Genet.*, **8**, 673-682.

44 Schmidt, T., Lindenberg, K.S., Krebs, A., Schols, L., Laccone, F., Herms, J., Rechsteiner, M., Riess, O. and Landwehrmeyer, G.B. (2002) Protein surveillance machinery in brains with spinocerebellar ataxia type 3: redistribution and differential recruitment of 26S proteasome subunits and chaperones to neuronal intranuclear inclusions. *Ann. Neurol.*, **51**, 302-310.

45 Gunawardena, S., Her, L.S., Brusch, R.G., Laymon, R.A., Niesman, I.R., Gordesky-Gold, B., Sintasath, L., Bonini, N.M. and Goldstein, L.S. (2003) Disruption of axonal transport by loss of huntingtin or expression of pathogenic polyQ proteins in *Drosophila*. *Neuron*, **40**, 25-40.

46 Higuchi, M., Tomioka, M., Takano, J., Shirotani, K., Iwata, N., Masumoto, H., Maki, M., Itoharu, S. and Saido, T.C. (2005) Distinct mechanistic roles of calpain and caspase activation in neurodegeneration as revealed in mice overexpressing their specific inhibitors. *J. Biol. Chem.*, **280**, 15229-15237.

47 Goll, D.E., Thompson, V.F., Li, H., Wei, W. and Cong, J. (2003) The calpain system. *Physiol. Rev.*, **83**, 731-801.

48 de Almeida, L.P., Zala, D., Aebischer, P. and Deglon, N. (2001) Neuroprotective effect of a CNTF-expressing lentiviral vector in the quinolinic acid rat model of Huntington's disease. *Neurobiol. Dis.*, **8**, 433-446.

49 Zala, D., Benchoua, A., Brouillet, E., Perrin, V., Gaillard, M.C., Zurn, A.D., Aebischer, P. and Deglon, N. (2005) Progressive and selective striatal degeneration in primary neuronal cultures using lentiviral vector coding for a mutant huntingtin fragment. *Neurobiol. Dis.*, **20**, 785-798.

50 Carter, R.J., Lione, L.A., Humby, T., Mangiarini, L., Mahal, A., Bates, G.P., Dunnett, S.B. and Morton, A.J. (1999) Characterization of progressive motor deficits in mice transgenic for the human Huntington's disease mutation. *J. Neurosci.*, **19**, 3248-3257.

LEGENDS TO FIGURES

Figure 1. BDA-410 inhibits calpains activity and decreases mutant ataxin-3 levels in vitro. *A*, Chemical structure of BDA-410. Representative western-blot analysis of cerebellar granule neurons three weeks after infection with lentiviral vectors encoding for wild-type ataxin-3 (ATX-3 27Q) or mutant ataxin-3 (ATX-3 72Q). One day after infection, cells were incubated with BDA-410 (50 or 100 nM) or DMSO. Non-infected cultures were used as a control (\emptyset). Membrane was incubated with *B*, spectrin antibody (MAB1622) or *C*, ataxin-3 antibody (Ab 1H9). *D*, Densitometric quantification of calpain cleaved spectrin (150/145 kDa fragments) level relative to tubulin (clone SAP.4G5), shown in panel B (n=9, \emptyset vs 27Q DMSO *P<0.05; \emptyset vs 72Q DMSO *P<0.05; 72Q DMSO vs 72Q BDA-410 100 nM #P=0.05). *E*, Densitometric quantification of full-length ataxin-3 level relative to actin (clone AC-74), shown in panel C (n=9, 72Q DMSO vs 72Q BDA-410 100 nM *P<0.05).

Figure 2. BDA-410 decreased ataxin-3 fragmentation in vivo. Western-blot of mice four weeks post-injection of lentiviral vectors encoding for wild-type ataxin-3 (ATX-3 27Q; left hemisphere) and mutant ataxin-3 (ATX-3 72Q; right hemisphere) in the striatum after daily gavage of vehicle (1% Tween80 saline; n=4) or BDA-410 (n=4). Depicted are blots of a pool of 4 animals for each condition using several antibodies to detect different epitopes of ataxin-3 protein: *A*, Ab 1H9, which recognizes amino acids E214-L233; *B*, Ab 1C2, specific for the polyglutamine stretch, present at the C-terminal of ataxin-3; and *C*, Ab myc, which recognizes myc tag located at the N-terminal of mutant ataxin-3. *D-F*, Densitometric quantification of ~26kDa fragment, ~34kDa fragment and full-length levels of ataxin-3, using Ab 1H9, relative to actin (n=4, *P<0.05, **P<0.01).

Figure 3. BDA-410 inhibits mutant ataxin-3 aggregation in vivo. Immunohistochemical analysis of mice eight weeks post-injection of lentiviral vectors encoding for mutant ataxin-3 (ATX-3 72Q) in the striatum after daily gavage of vehicle (1% Tween80 saline; n=6) or BDA-410 (n=6) using an *A-D*, anti-ataxin-3 antibody (Ab 1H9) or *E-F*, anti-ubiquitin antibody (Dako). Quantification of the absolute number of *G*, ataxin-3 intranuclear inclusions (**P<0.01); graph related to panel A-D. Values are expressed as mean \pm standard error of the mean.

Figure 4. Mutant ataxin-3 aggregates of specific size have different toxic properties.

Immunohistochemical analysis of mice eight weeks post-injection of lentiviral vectors encoding for mutant ataxin-3 (ATX-3 72Q) in the striatum after daily gavage of vehicle (1% Tween80 saline; n=6) or BDA-410 (n=6). Upper panel: Coronal sections were stained for *A,D*, mutant ataxin-3 (ATX-3 72Q, Ab 1H9, green), *B,E*, ubiquitin (Dako, red), nuclear marker (DAPI, blue). *C,F*, merge images of *A* and *B* or *D* and *E*, respectively. Lower panel: Coronal sections were stained for *G,J*, mutant ataxin-3 (ATX-3 72Q, Ab 1H9, red), *H,K*, cleaved caspase-3 (Asp 175, green), nuclear marker (DAPI, blue). *I,L*, merge images of *G* and *H* or *J* and *K*, respectively. *M*, Analysis of mutant ataxin-3 intranuclear inclusions diameter. Graph related to upper panel. *N*, Analysis of mutant ataxin-3 intranuclear inclusions diameter, with (+) or without (-) colocalization with cleaved caspase-3 (***P*<0.0001). Graph related to lower panel. *O*, Cytotoxicity, measured by cleaved caspase-3. Results are presented as a percentage of mutant ataxin-3 positive cells co-expressing cleaved caspase-3 (**P*<0.05). Graph related to lower panel.

Figure 5. BDA-410 prevents cell injury and striatal degeneration. Immunohistochemical analysis of mice eight weeks post-injection of lentiviral vectors encoding for mutant ataxin-3 (ATX-3 72Q) in the striatum after daily gavage of vehicle (1% Tween80 saline; n=6) or BDA-410 (n=6) *A-D*, using an anti-DARPP-32 antibody. *C,D* are a higher magnification of *A,B*. *E,F*, Cresyl violet staining using the same experimental paradigm. *G*, Quantification analysis of the DARPP-32 depleted volume in the mice brains (**P*<0.05). *H*, Quantification analysis of the pycnotic nuclei visible in treated and vehicle groups on cresyl violet-stained sections (***P*<0.001).

Figure 6. BDA-410 alleviates motor disabilities. Behaviour analysis of mice two, seven and ten weeks post-injection of lentiviral vectors encoding for mutant ataxin-3 (ATX-3 72Q) in the cerebellum after daily gavage of vehicle (1% Tween80 saline; n=6) or BDA-410 (n=6). Non-injected mice (Ø) of the same age were used as a control. *A*, Balance and motor coordination measured by the mean latency time for each animal over time to cross all the raised beams (Ø vs vehicle **P*<0.05; Ø vs BDA-410 NS=non-significant; vehicle vs BDA-410 #*P*<0.05) two and seven weeks post-injection. *B*, Analysis of mice neuromuscular function using a grip strength test (Ø vs vehicle **P*<0.05; Ø vs BDA-410 NS=non-significant; vehicle vs BDA-410 #*P*=0.05) ten

weeks post-injection. Footprint pattern analysis in *C*, stride length ten weeks post-injection.

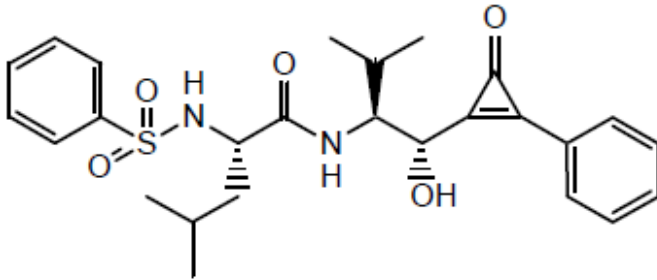
Values are expressed as mean \pm SEM.

Figure 7. BDA-410 prevents cell loss. Histological analysis of mice thirteen weeks post-injection of lentiviral vectors encoding for mutant ataxin-3 (ATX-3 72Q) in the cerebellum after daily gavage of vehicle (1% Tween80 saline; n=3) or BDA-410 (n=3). Non-injected mice (\emptyset) of the same age were used as a control. Midsagittal cresyl violet staining depicting *A-C*, the cerebellum and *D-F*, the molecular layer of lobule V. Immunohistochemical analysis using the same experimental paradigm stained for *G-I*, calbindin (Ab1778, green). Quantification analysis of lobule V *J*, volume (\emptyset vs vehicle **P<0.01; \emptyset vs BDA-410 *P<0.05; vehicle vs BDA-410 #P<0.05), *K*, molecular layer width (\emptyset vs vehicle **P<0.01) and *L*, Purkinje cells number (\emptyset vs vehicle *P<0.05). Values are expressed as mean \pm SEM.

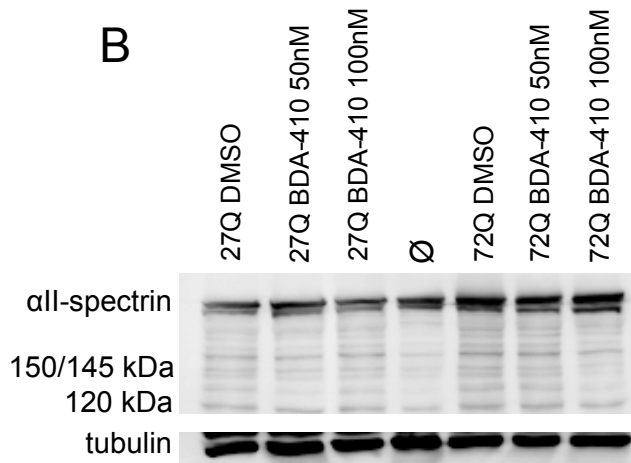
ABBREVIATIONS

Ab - antibody; ATX-3 - ataxin-3; DAPI - 4',6-diamino-2-phenylindole; DARPP-32 - Dopamine- and cyclic AMP-regulated phosphoprotein of 32 kDa; CAG - Cytosine-adenine-guanine; MJD - Machado-Joseph disease; CNS - Central nervous system; UPS - ubiquitin proteasome system

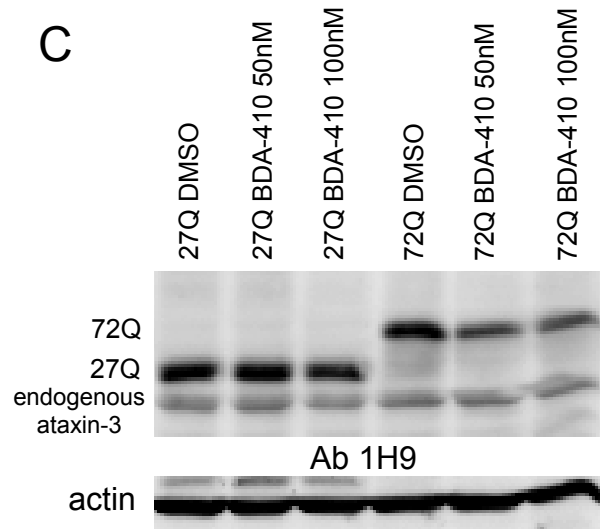
A



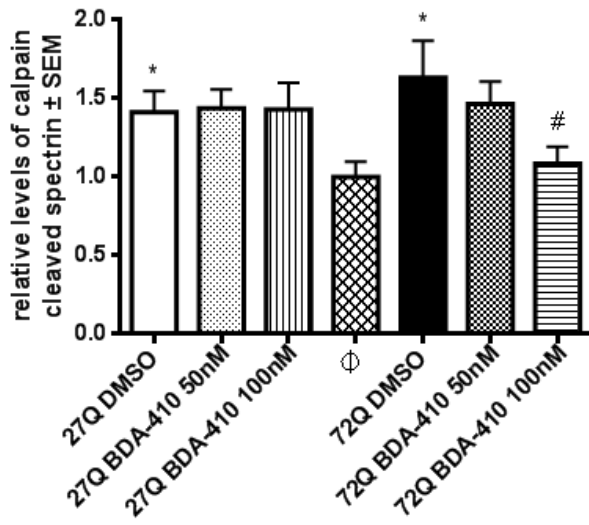
B



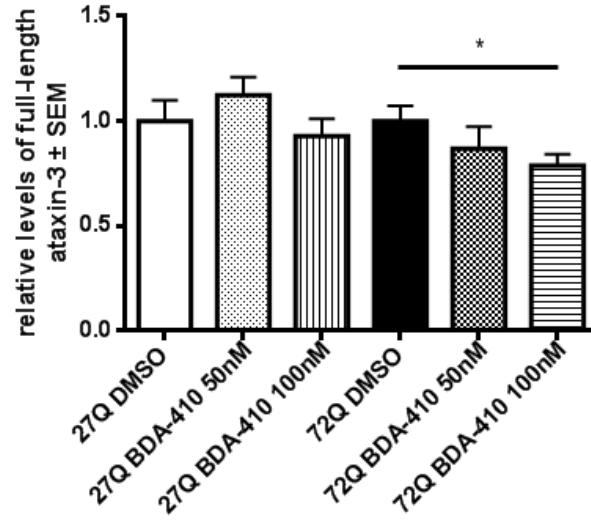
C

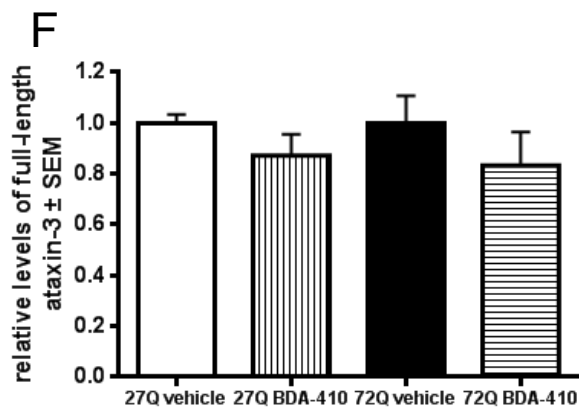
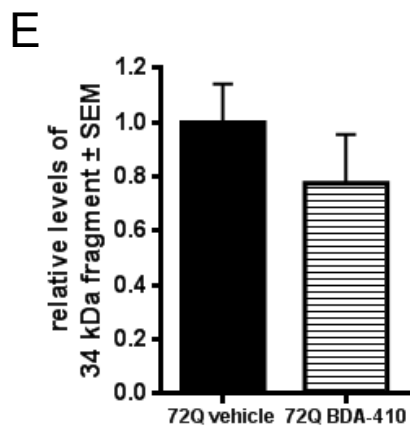
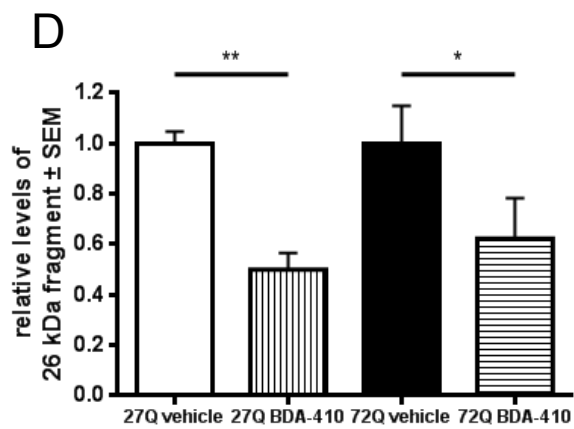
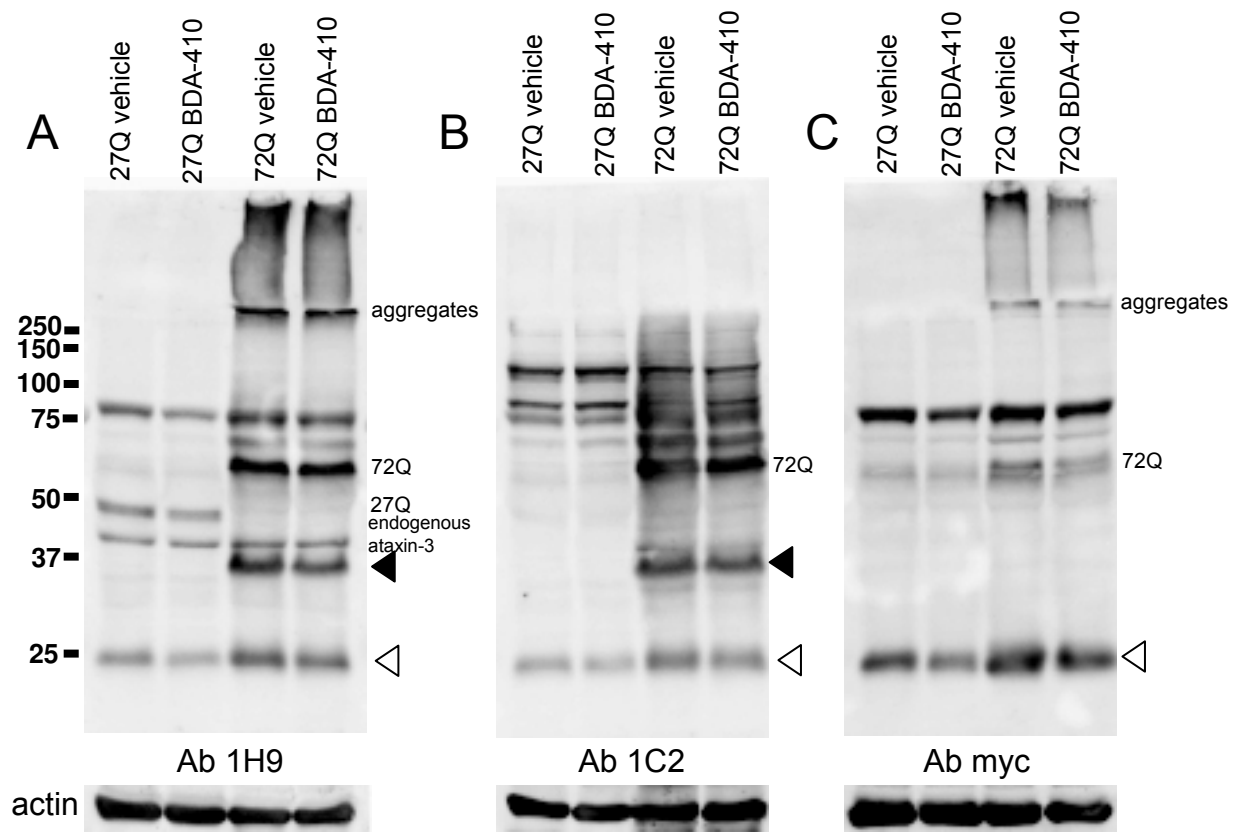


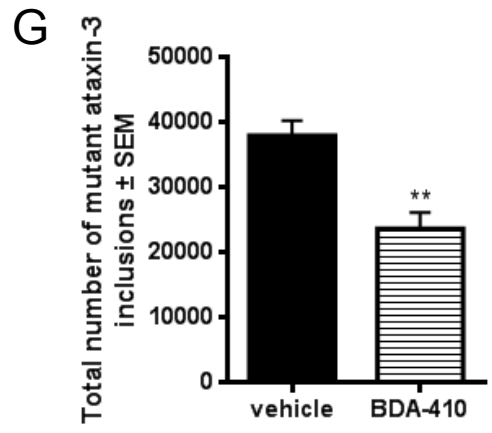
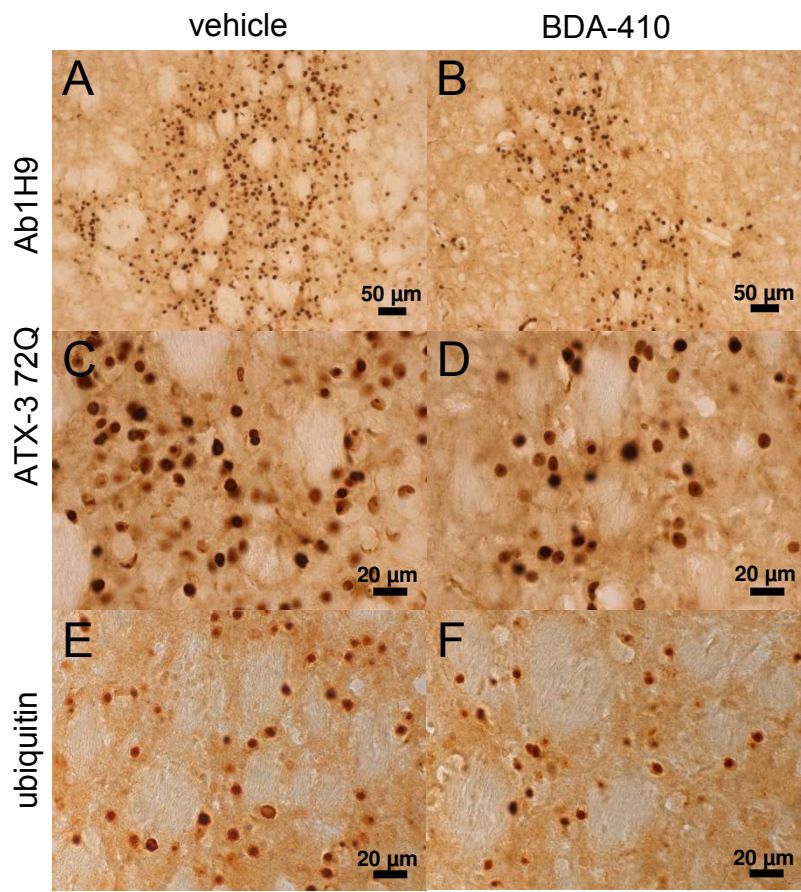
D

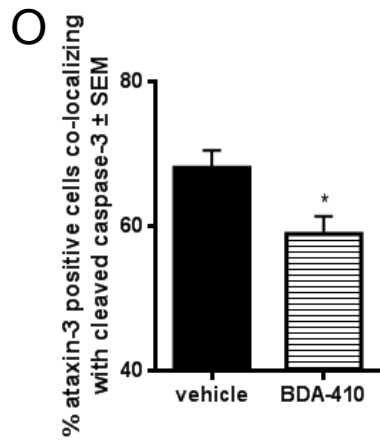
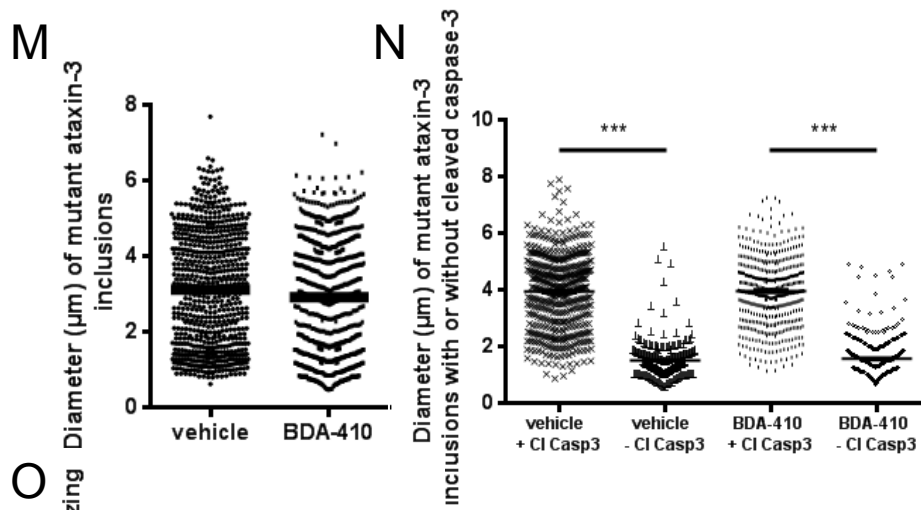
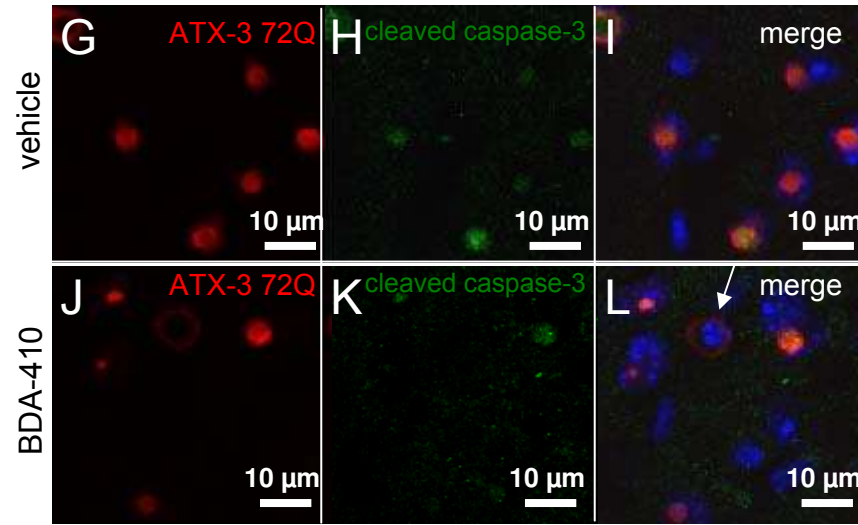
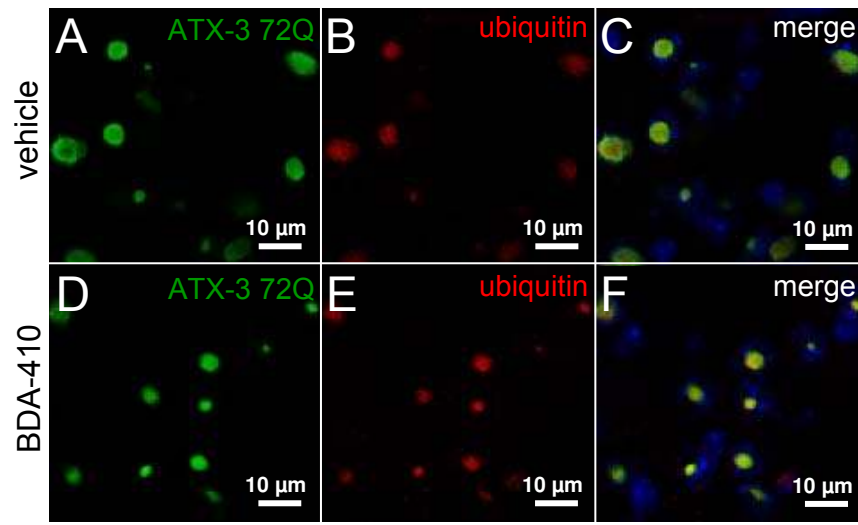


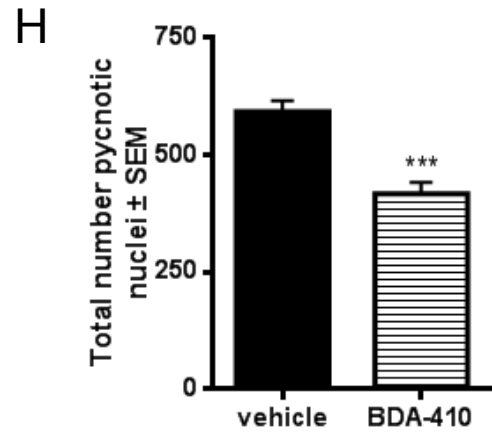
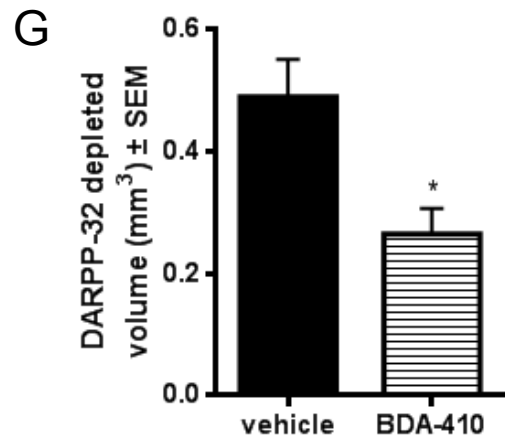
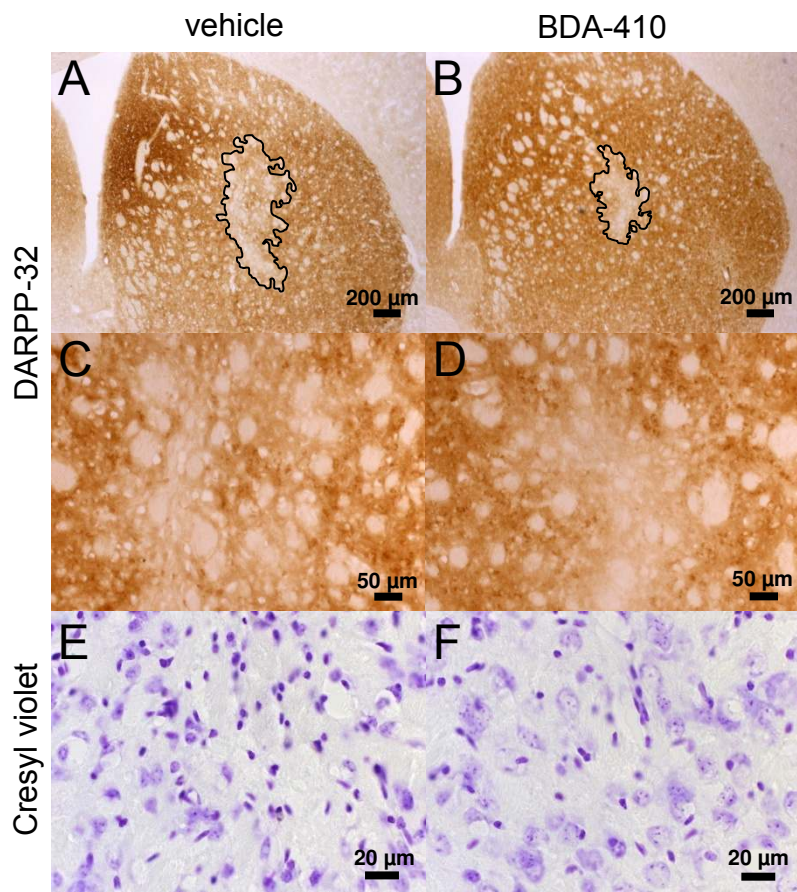
E

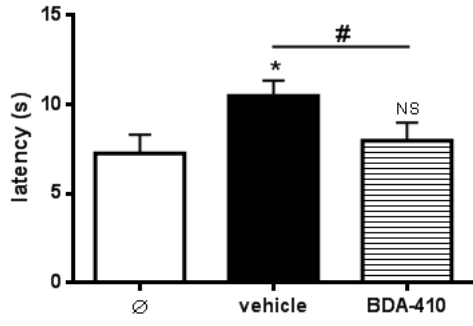
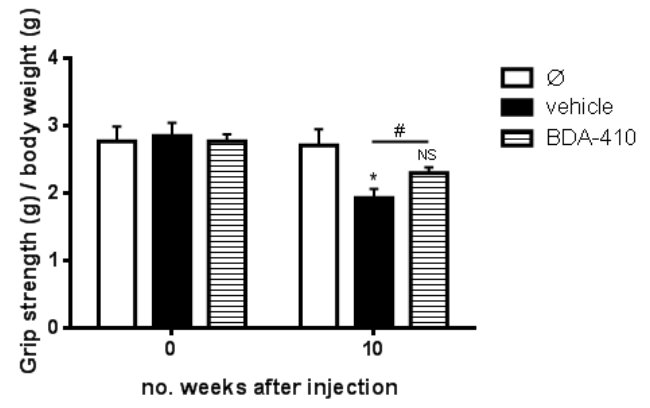










A**B****C**